Potent in vitro anti-*Trypanosoma cruzi* activity of pyridine-2-thiol *N*-oxide metal complexes having an inhibitory effect on parasite-specific fumarate reductase

**Marisol Vieites · Pablo Smircich · Beatriz Parajón-Costa · Jorge Rodríguez · Verónica Galaz ·
Claudio Olea-Azar · Lucía Otero · Gabriela Aguirre · Hugo Cerecetto · Mercedes González ·
Alicia Gómez-Barrio · Beatriz Garat · Dinorah Gambino**

Abstract In the search for new therapeutic tools against
Chagas disease (American trypanosomiasis) palladium and
platinum complexes of the bioactive ligand pyridine-2-
thiol *N*-oxide were exhaustively characterized and evalu-
ated in vitro. Both complexes showed high in vitro growth
inhibition activity (IC_{50} values in the nanomolar range)
against *Trypanosoma cruzi*, the causative agent of the
disease. They were 39–115 times more active than the
antitrypanosomal drug Nifurtimox. The palladium complex
showed an approximately threefold enhancement of the
activity compared with the parent compound. In addition,
owing to their low unspecific cytotoxicity on mammalian
cells, the complexes showed a highly selective antiparasite
activity. To get an insight into the mechanism of action of
these compounds, DNA, redox metabolism (intraparasite
free-radical production) and two parasite-specific enzymes
absent in the host, namely, trypanothione reductase and
NADH-fumarate reductase, were evaluated as potential
parasite targets. Additionally, the effect of metal coordi-
nation on the free radical scavenger capacity previously
reported for the free ligand was studied. All the data
strongly suggest that trypanocidal action of the complexes
could mainly rely on the inhibition of the parasite-specific
enzyme NADH-fumarate reductase.

M. Vieites · L. Otero · D. Gambino (✉)
Cátedra de Química Inorgánica,
Facultad de Química,
Universidad de la República,
Gral. Flores 2124, C. C. 1157,
11800 Montevideo, Uruguay
e-mail: dgambino@fq.edu.uy

P. Smircich · B. Garat
Laboratorio de Interacciones Moleculares,
Facultad de Ciencias,
Universidad de la República,
Iguá 4225, 11400 Montevideo, Uruguay

B. Parajón-Costa
Centro de Química Inorgánica
(CEQUINOR/CONICET-UNLP),
C.C. 962, Facultad de Ciencias Exactas,
Universidad Nacional de La Plata,
1900 La Plata, Argentina

J. Rodríguez · V. Galaz · C. Olea-Azar
Departamento de Química Inorgánica y Analítica,
Facultad de Ciencias Químicas y Farmacéuticas,
Universidad de Chile,
Casilla 233, Santiago, Chile

G. Aguirre · H. Cerecetto · M. González
Laboratorio de Química Orgánica,
Facultad de Química–Facultad de Ciencias,
Universidad de la República,
Iguá 4225, 11400 Montevideo, Uruguay

A. Gómez-Barrio
Departamento de Parasitología,
Facultad de Farmacia,
Universidad Complutense,
28040 Madrid, Spain

Introduction

According to the WHO, infectious and parasitic diseases are major causes of human disease worldwide [1, 2]. Although they represent a tremendous burden compared with other communicable diseases that receive a higher level of attention from health systems, a group of parasitic and infectious diseases, called neglected diseases, has been characterized by historically low investment by the pharmaceutical industry. Often, the most affected populations are also the poorest and the most vulnerable and they are found mainly in tropical and subtropical areas of the world. In particular, parasitic diseases represent a major health problem in Latin America. Among neglected diseases, Chagas disease (American trypanosomiasis) is the largest parasitic disease burden in the American continent, affecting approximately 20 million people from the southern USA to southern Argentina [1, 3]. The morbidity and mortality associated with this disease in America are more than 1 order of magnitude higher than those caused by malaria, schistosomiasis or leishmaniasis. The disease is caused by the flagellate protozoan parasite *Trypanosoma cruzi*, which is mainly transmitted to humans in two ways, either by blood-sucking reduviid insects of the Triatominae family that deposit their infective feces on the skin of the host at the time of biting, or directly by transfusion of infected blood. Humans and a large number of species of domestic and wild animals constitute the reservoir.

Trypanosomes diverged very early from the common eukaryotic lineage, and their biochemistry differs in numerous aspects from that of mammalian cells. Despite the progress achieved in the study of the biochemical and physiological processes of *T. cruzi*, in which several crucial enzymes for parasite survival, absent in the host, have been identified as potential new drug targets, the chemotherapy of this parasitic infection remains underdeveloped and no effective method of immune prophylaxis is available. The treatment is based on old and quite unspecific nitroaromatic drugs that have significant activity only in the acute phase of the disease and, when associated with long-term treatments, give rise to severe side effects [4–8]. In the search for a pharmacological control of Chagas disease, metal complexes appear to be a promising new approach [5, 9–12]. A successful strategy has been based on the synthesis of complexes combining ligands bearing antitrypanosomal activity and pharmacologically active metals. The metal compounds obtained could act through dual or even multiple mechanisms of action by combining the pharmacological properties of both the ligand and the metal,

leading to a synergistic or at least an additive effect [11, 12]. The development of single agents that provide maximal antiprotozoal activity by acting against multiple parasitic targets could diminish host toxic effects by lowering therapeutic dose and/or circumventing the development of drug resistance [13]. Leading work performed by Sánchez-Delgado et al. [11, 12] resulted in metal complexes of clotrimazole and ketoconazole intended for antitrypanosome therapy. Synergistic effects were observed in most of the cases. We have also been successfully working on the development of new therapeutic tools for the treatment of Chagas disease using this strategy [14, 15]. A series of vanadyl bioactive compounds of aromatic amine *N*-oxides has been developed and exhaustively studied [14]. The anti-*T. cruzi* activity of two novel series of palladium compounds has been evaluated in vitro and some aspects related to their possible synergistic effect and dual or even multiple mechanisms of action have been investigated [15].

Based on this approach, in this work we propose to test coordination compounds of the bioactive ligand pyridine-2-thiol *N*-oxide (2-mercaptopyridine *N*-oxide, mpo; Fig. 1) as potential antitrypanosomal agents and to get an insight into their mechanism of action.

Mpo blocks *T. cruzi*'s growth in culture and in infected mammalian myoblasts, affecting all stages of the life cycle of the parasite without affecting mammalian cells and showing low 50% inhibitory concentration (IC_{50}) values [16]. Although it may have other intracellular targets, it inhibits the parasite-specific enzyme NADH-fumarate reductase, the enzyme responsible for the conversion of fumarate to succinate [16]. Succinate is one of the main respiratory substrates and is therefore required by the parasite for energy production. In addition, it may be used as a sink for the elimination of excessive reduction equivalents since lactic dehydrogenase is absent in trypanosomatids. The lack of NADH-fumarate reductase in mammalian cells provides an interesting target against Chagas disease. In addition, mpo, as other heterocyclic amine *N*-oxides do, could release, by bioreduction in the cell, radical species, mainly hydroxyl radical, that could cause cellular damage [17, 18].

As a first stage, palladium and platinum were selected as central metals because of the postulated metabolic
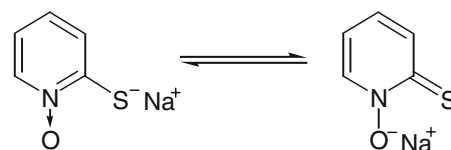
Fig. 1 Pyridine-2-thiol *N*-oxide sodium salt in its two tautomeric forms

similarities between tumor cells and *T. cruzi*'s cells [11]. Compounds of both metals have proven their effect on tumor cells and their ability to bind DNA as the main antitumoral mechanism of action [19–21]. In addition, some palladium and platinum compounds have shown anti-*T. cruzi* activity acting through different mechanisms, like DNA interaction and irreversible inhibition of *T. cruzi*'s specific flavoenzyme trypanothione reductase (TR) [5, 15, 22–25]. In trypanosomes, the nearly ubiquitous glutathione/glutathione reductase system is replaced by trypanothione and TR. The absence of trypanothione in the mammalian host and the uniqueness of the parasite thiol metabolism together with the essential role of TR in the defense of trypanosomatids against oxidative stress render TR an attractive drug target [5, 26].

Although the interaction of mpo with transition metal cations has been extensively investigated, there is little information about the redox properties of its coordination compounds. The Fe^{II}, Co^{II}, Ni^{II} and Mn^{II} complexes have been briefly investigated by cyclic voltammetry and only a detailed study of the oxovanadium(IV) complex has been performed [27].

In this work we exhaustively characterized Pd(mpo)$_2$ and Pt(mpo)$_2$ complexes, even though the compounds had been previously synthesized, by Fourier transform IR (FTIR), Raman and NMR spectroscopies [28–30]. In addition, owing to the potential relevance of the electrochemical behavior of metal-based drugs in determining biological activity, a detailed study of both complexes was performed by cyclic voltammetry. Further, free-radical production by electrolytic reduction was studied by electronic spin resonance (ESR). In vitro activity against *T. cruzi* was determined and unspecific cytotoxicity on mammalian cells was evaluated. Furthermore, to get an insight into the mechanism of the antitrypanosomal action of these compounds, their effect on some probable parasite targets was evaluated. In this sense and taking into account the already mentioned antecedents, studies on DNA interaction, intraparasite free-radical production and inhibition of the parasite-specific enzyme TR, absent in the host, were performed. Additionally, the effects of metal coordination on some biological properties reported for the ligand, namely, free radical scavenger capacity and inhibition of the parasite-specific enzyme NADH-fumarate reductase, were studied.

Materials and methods

Materials

All common laboratory chemicals were purchased from commercial sources and used without further purification.

The sodium salt of mpo (Na mpo), [PdCl$_2$] and K$_2$[PtCl$_4$] were commercially available.

Syntheses of the complexes

Pd^{II}(mpo)$_2$

The palladium complex was prepared through a modification of a previously reported procedure [28]. [PdCl$_2$] (50 mg, 0.28 mmol) and Na mpo (168 mg, 1.13 mmol), molar ratio 1:4, were heated under reflux in methanol/acetonitrile (1:1, v/v) (23 mL) for 5 h. By slow evaporation of the solution, brown–reddish single crystals were obtained. Yield: 22.8 mg, 21%. Anal (%) calcd for C$_{10}$H$_8$N$_2$O$_2$PdS$_2$: C, 33.48; H, 2.25; N, 7.81. Found: C, 33.36; H, 1.92; N, 7.89. IR (KBr)/Raman (cm^{-1}): 1,247 s/1,245 s, v(N–O); 821 s/820 m, δ(N–O); 708 s/707 m, v(C–S). IR (CsI, 400–200 cm^{-1}) (cm^{-1}): 442 w, 392 w, 313 w.

Pt^{II}(mpo)$_2$

The platinum complex was prepared by refluxing K$_2$[PtCl$_4$] (50 mg, 0.12 mmol) and Na mpo (72 mg, 0.48 mmol), molar ratio 1:4, in methanol/acetonitrile (1:1) (10 mL) for 5 h. Yellow single crystals were obtained by slow evaporation of the solution. Yield: 11.2 mg, 32%. Anal (%) calcd for C$_{10}$H$_8$N$_2$O$_2$PtS$_2$: C, 26.85; H, 1.80; N, 6.26. Found: C, 26.87; H, 1.72; N, 6.10. IR (KBr)/Raman (cm^{-1}): 1,250 s/1,251 s, v(N–O); 814 s/823 m, δ(N–O); 711 s/713 m, v(C–S). IR (CsI, 400–200 cm^{-1}) (cm^{-1}): 434 w, 386 w, 300 w.

Physicochemical characterization

C, H and N analyses were performed with a Carlo Erba model EA1108 elemental analyzer. FTIR spectra (4,000–400 and 500–200 cm^{-1}) of the complexes and the free ligand were measured either as KBr or as CsI pellets with a Bomen FTIR model M102 instrument. Raman spectra were scanned with the FRA 106 accessory of a Bruker IF 66 FTIR spectrophotometer. The 1,064 nm radiation of a Nd:YAG laser was used for excitation and 50–60 scans were routinely accumulated. ^{1}H NMR and ^{13}C NMR spectra of the free ligand and of the complexes were recorded with a Bruker DRX-400 instrument (at 400 and 100 MHz, respectively). Experiments were performed at 30 °C in dimethyl-d_6 sulfoxide (DMSO-d_6)–D$_2$O (9:1). The stability of the complexes in such media over at least 24 h was determined by NMR. Neither free ligand nor coordinated DMSO was detected. Two-dimensional heteronuclear correlation experiments, namely, heteronuclear multiple quantum correlation (HMQC) and heteronuclear multiple bond correlation (HMBC), were performed with the same

instrument. Tetramethylsilane was used as the internal standard. Chemical shifts are reported in parts per million. The crystal parameters of single crystals of both complexes were compared with those previously reported [28, 30].

The electrochemical behavior of the complexes was studied by cyclic voltammetry. Cyclic voltammograms were obtained with a PAR potentiostat/galvanostat model 263A controlled by the 270/250 software (EG&G Princeton Applied Research). A printer and a standard electrochemical three-electrode cell of 10-mL volume completed the system. A glassy carbon disc was employed as the working electrode. A platinum wire was used as the counter electrode, while $Ag/10^{-3}$ M $AgNO_3$ in acetonitrile/0.1 M tetrabutylammonium hexafluorophosphate [$(TBA)PF_6$] was used as the reference electrode. This electrode was calibrated against the $[Fe(C_5H_5)_2]/[Fe(C_5H_5)_2]^+$ redox couple, for which a potential of +0.4 V versus the normal hydrogen electrode (NHE) was assumed [31, 32]. All potentials reported are referred to the NHE in volts. The measurements were performed in 10^{-3} M dimethylformamide (DMF) solutions containing 0.1 M $(TBA)PF_6$, as the supporting electrolyte. High-purity DMF (Baker, spectroscopic grade) was dried over 4-Å molecular sieves (Merck) and used without further purification. $(TBA)PF_6$ was purchased from Fluka (electrochemical grade) and used as received. Solutions were deoxygenated via purging with extrapure nitrogen for 15 min prior to the measurements. A continuous gas stream was passed over the solution during the measurements.

The complexes were also tested for their capability to produce free radicals in reductive conditions. ESR spectra of the free radicals obtained by electrolytic reduction were recorded in the X band (9.85 GHz) using a Bruker ECS 106 spectrometer with a rectangular cavity and 50-kHz field modulation. Radicals of mpo and of the complexes were generated by electrolytic reduction in situ in 10^{-3} M DMSO solutions at room temperature under a nitrogen atmosphere. The ESR conditions were previously established by performing cyclic voltammetry on a Metrohm 693 VA instrument with 0.1 M tetrabutylammonium perchlorate as the supporting electrolyte using a three-electrode cell. A dropping-mercury electrode was used as the working electrode, a platinum wire as the auxiliary electrode, and saturated calomel electrode as the reference electrode. Simulations of the ESR spectra were made using Simfonia version 1.25. The hyperfine splitting constants were estimated to be accurate within 0.05 G [33]. Full geometry optimizations, in vacuo, of mpo in spin-paired forms were carried out using the AM1 semiempirical method. The theoretical hyperfine constants were calculated using the open-shell UB3LYP method with the 6-31G* basis set.

In vitro anti-*T. cruzi* activity

Handling of live *T. cruzi* was done according to established guidelines [34]. The epimastigote form of the parasite Tulahuen 2 strain was grown at 28 °C in an axenic medium (brain–heart infusion tryptose), complemented with 10% fetal calf serum. Cells from a 5-day-old culture were inoculated into 50 mL of fresh culture medium to give an initial concentration of 1×10^6 cells per milliliter. Cell growth was followed by measuring daily the absorbance A of the culture at 600 nm for 11 days. Before inoculation, the medium was supplemented with 5 μM concentration of compounds from a stock DMSO solution. The final DMSO concentration in the culture medium never exceeded 0.4% (v/v) and had no effect by itself on the proliferation of the parasites (no effect on epimastigote growth was observed with the presence of up to 1% DMSO in the culture medium). The compounds' ability to inhibit the growth of the parasite was evaluated, in triplicate, in comparison with that of the control (no drug added to the medium). The control was run in the presence of 0.4% DMSO and in the absence of any drug. The percentage of growth inhibition (PGI) was calculated as follows: $\text{PGI} = \{1 - [(A_p - A_{0p})/(A_c - A_{0c})]\} \times 100$, where $A_p = A_{600}$ of the culture containing the drug at day 5; $A_{0p} = A_{600}$ of the culture containing the drug just after addition of the inocula (day 0); $A_c = A_{600}$ of the culture in the absence of any drug (control) at day 5; $A_{0c} = A_{600}$ in the absence of the drug at day 0. Nifurtimox (Nfx) was used as the reference trypanocidal drug. Dose–response curves were recorded and the IC_{50} values were assessed [15].

Cytotoxicity on macrophages

J774 macrophages were seeded (70,000 cells per well) in 96-well flat-bottom microplates (Nunclon) with 200 μL of RPMI 1640 medium supplemented with 20% heat-inactivated fetal calf serum. The cells were allowed to attach for 24 h in a humidified 5% CO_2/95% air atmosphere at 37 °C. Then, the cells were exposed to the compounds (1, 0.5, 0.25, 0.1, 0.05 and 0.025 μg mL^{-1}) for 24 h. Afterwards, the cells were washed with phosphate-buffered saline and incubated at 37 °C with 0.4 mg mL^{-1} 3-(4,5-dimethylthiazol-2-yl)-2,5-diphenyltetrazolium bromide for 60 min. Then, formazan was dissolved with DMSO (100 μL) and absorbances (A) at 595 nm were measured. Each concentration was assayed three times and six growth controls were used in each test. Cytotoxicity percentages were determined as $C(\%) = 100 - (A_d - A_{dm})/(A_c - A_{cm}) \times 100$, where A_d is the mean of A_{595} of wells with macrophages and different concentrations of the compounds; A_{dm} is the mean of A_{595} of wells with different concentrations of the compounds in the

medium; A_c is the growth control and A_{cm} is the mean of A_{595} of wells with only medium [35].

Calf thymus DNA interaction experiments

The complexes were tested for their DNA interaction ability using native calf thymus DNA (CT DNA) (type I) by a modification of a previously reported procedure [36]. CT DNA (50 mg) was dissolved in water (30 mL) (overnight) and the concentration per nucleotide was determined by UV absorption spectroscopy using a molar absorption coefficient of 6,000 M^{-1} cm^{-1} at 260 nm. Solutions of the complexes in DMSO (spectroscopy grade) (1 mL, 10^{-3} M) were incubated at 37 °C with a solution of CT DNA (1 mL) for 96 h. DNA/complexes mixtures were exhaustively washed to eliminate the unreacted complex. Quantification of bound metal was done by atomic absorption spectroscopy with a PerkinElmer 380 spectrometer. Standards were prepared by diluting a metal standard solution.

Plasmid DNA interaction studies

Plasmid DNA interaction studies for both complexes were performed using a previously described procedure [37]. Plasmid DNA (pBSK II BlueScript, Stratagene; 300 ng per reaction) was obtained and purified according to standard techniques [38]. Briefly, *Escherichia coli* XL1 cells were transformed with pBSK II. Transformation was verified by polymerase chain reaction and plasmidic DNA was purified (Qiagen Plasmid Maxi Kit). Spectrophotometric DNA quantification was carried out assuming a molar absorption coefficient at 260 nm of 0.02 μg^{-1} mL cm^{-1}.

Complexes were dissolved in 1% DMSO–H_2O. The purified DNA was incubated in the presence of the complexes for 24 h at 37 °C [final volume 20 μL, reaction buffer 10 mM tris(hydroxymethyl)aminomethane (Tris) hydrochloride, 0.1 mM ethylenediaminetetraacetic acid disodium salt (EDTA), pH 7.5]. No effect on DNA due to DMSO addition was observed even for higher concentrations than those used for dissolution purposes [37]. During the 24-h incubation period involved in the gel electrophoresis experiments no appreciable hydrolysis or decomposition of the complexes was detected by NMR in DMSO–H_2O medium. Various molar ratios r_i (r_i is the ratio of number of moles of the complex to the number of moles of the base pair) in the range 0.5–4.0 were assayed. After incubation, reactions were stopped by the addition of loading buffer (25% bromophenol blue, 50% glycerol, 25 mM EDTA, pH 8.0). In all cases, samples were electrophoresed in 0.7% agarose buffered with 90 mM Tris–borate at 70 V for 2 h. The gel was subsequently stained with an ethidium bromide solution (0.5 μg mL^{-1}) for 30 min and destained in water for 20 min.

Otherwise, the gel contained 0.5 μg mL^{-1} ethidium bromide. Bands were visualized under UV light and quantified using OneDSCAN.

Intraparasite free-radical production

The free radical production capacity of the new complexes was studied in the parasite by ESR using 5,5-dimethyl-1-pirroline *N*-oxide (DMPO) for detecting free-radical species with a short half-life. Each compound tested was dissolved in DMF (spectroscopy grade) (approximately 1 mM) and the solution was added to a mixture containing the epimastigote form of *T. cruzi* (Dm28c strain, 4–8 mg mL^{-1} protein) and 100 mM DMPO in 50 mM phosphate buffer pH 7.4. The mixture was transferred to a 50-μL capillary. ESR spectra were recorded in the X band (9.85 GHz) using a Bruker ECS 106 spectrometer with a rectangular cavity and 50-kHz field modulation. All the spectra were registered on the same scale after 15 scans.

Free radical scavenger capacity: ORAC$_{FL}$ assay

An LS 50B luminescence spectrometer (PerkinElmer, Boston, MA, USA), a DC1–B3 heating circulator bath (Haake Fisons, Karlsruhe, Germany), quartz cuvettes and 490-P excitation and 515-P emission filters were used. The ORAC method of Ou et al. [39] was modified as follows. The reaction was carried out in 75 mM phosphate buffer (pH 7.4) and the final reaction volume was 3,000 μL. A mixture of the compounds studied (15, 30, 45, 60 μL; 0.5–2.0 μM final concentrations) and fluorescein (FL) (215 μL; 70 nM final concentration) solutions was preincubated in a cuvette for 30 s at 60 °C. After the rapid addition of 2,2′-azobis(2-methylpropionamidine) dihydrochloride (AAPH) solution (240 μL; 12 mM final concentration) the fluorescence was recorded at 60 °C every minute for 12 min. As a blank FL and AAPH in phosphate buffer was employed and eight calibration solutions using 6-hydroxy-2,5,7,8-tetramethylchroman-2-carboxylic acid (Trolox) (1–8 μM, final concentration) as an antioxidant positive control were also employed in each assay. All the reaction mixtures were prepared in duplicate, and at least three independent assays were performed for each sample. Blank and antioxidant curves (fluorescence vs. time) were first normalized by dividing the original data by the value for the fluorescence at $t = 0$ s. From the normalized curves, the area under the fluorescence decay curve (AUC) was calculated as

$$AUC = 1 + \sum_{i=1}^{i=12} \frac{f_i}{f_0}$$

where f_0 is the initial fluorescence reading at 0 min and f_i is the fluorescence reading at time i. The net AUC corresponding to each sample was calculated by subtracting the

AUC corresponding to the blank. Regression equations between the net AUC and antioxidant concentration were calculated for all the samples. ORAC$_{FL}$ values were expressed as Trolox equivalents by using the standard curve calculated for each assay. The final results were expressed in micromoles of Trolox equivalent per micromole of sample [40].

T. cruzi TR inhibition assays

Recombinant TR activity was measured spectrophotometrically at 25 °C in TR assay buffer [40 mM *N*-(2-hydroxyethyl)piperazine-*N*′-ethanesulfonic acid (Hepes), 1 mM EDTA, pH 7.5] as previously described [41]. Stock solutions (4 mM) of the complexes and the free ligand were prepared in DMSO. The assay mixtures (1 mL) contained 100 μM NADPH, 100 μM trypanothione disulfide (TS$_2$) and various concentrations of the inhibitor. NADPH, enzyme and inhibitor were mixed. The reaction was started by adding TS$_2$ and the absorption decrease at 340 nm due to NADPH consumption was followed. Control assays contained the respective amount of DMSO instead of inhibitor [15].

T. cruzi NADH-fumarate reductase activity measurements

For the enzyme activity assays *T. cruzi* protein extracts were prepared as previously reported but introducing minor modifications [42]. Briefly, *T. cruzi* epimastigotes (Dm28c clone) were grown at 28 °C in liver infusion tryptose medium supplemented with 10% heat-inactivated fetal bovine serum [43]. Parasites (5×10^7 mL^{-1}) were harvested at 500 g and were resuspended in 0.23 M mannitol, 0.07 M sucrose, 5 mM Tris–HCl, pH 7.4 containing several protease inhibitors (10 μg mL^{-1} leupeptin, 10 μg mL^{-1} bestatin and 10 μg mL^{-1} pepstatin). Cell suspensions were homogenized in the presence of 0.1% Triton X-100 and 200 mM KCl on ice using a Potter–Elvehjem Teflon-glass homogenizer to disrupt the cell membranes and extract the enzyme. The preparation was immediately used to spectrophotometrically test NADH-fumarate reductase activity as the fumarate-dependent rate of NADH oxidation at 340 nm (molar absorption coefficient of 6.22 mM^{-1} cm^{-1}) using 250 μM NADH in buffer 30 mM Hepes pH 7.0 containing 125 mM KCl and 0.5 mM fumarate as previously described [44].

Results and discussion

The Pt–mpo complex was synthesized with high purity and good yield by a different route from that previously reported [29, 30]. Although Pd(mpo)$_2$ and Pt(mpo)$_2$ complexes had been previously synthesized, in this work an exhaustive description of the characterization results of the platinum complex by FTIR, Raman and NMR spectroscopies was performed and the results were compared with the corresponding results for the palladium complex [28, 30]. Most of the relevant IR and Raman vibration bands of both complexes were assigned (Table S1) [27, 45, 46]. The bands corresponding to v(N–O) and v(C–S) vibrations were assigned taking into account previous assignments for related compounds bearing the *N*-oxide or thiocarbonyl moieties [14, 15, 47, 48]. The v(N–O), δ(N–O) and v(C–S) bands shift after coordination to the metal in agreement with the bidentate coordination of the ligand through the oxygen of the N–O group and the sulfur, shown in the corresponding crystal structures [28, 30]. Bands corresponding to metal-to-ligand stretching modes were also identified in the low-wavenumber region (400–200 cm^{-1}) and were tentatively assigned to v(M–O) and v(M–S).
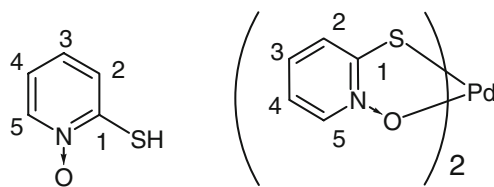
Table 1 shows the ^{1}H and ^{13}C NMR chemical shifts (δ) of the ligand and the complexes, and the chemical shift differences between them, expressed as $\Delta\delta$. The figure shows the numbering scheme. ^{1}H NMR integrations and signal multiplicities were in agreement with the proposed formula and structure. HMQC and HMBC experiments allowed the assignment of all the signals of the free ligand and the complexes investigated. When the ligand is coordinated to the Pd(II) or Pt(II) cations a deshielding effect of all the protons appears as the result of an electron withdrawal caused by coordination. However, a slight deshielding effect was observed for those protons that are located close to the coordinating atoms, protons 2 and 5, as the result of a shielding effect due to the presence of the O–metal–S neighboring entity. Upon coordination, the most distinguishing feature of the ^{13}C NMR spectra was the change in the chemical shift of carbon 1, which decreases from approximately 168 to 154–157 ppm. In disagreement with the previous spectroscopical report [28], the HMQC and HMBC experiments performed in this work allowed us to assign unequivocally the chemical shifts of carbons 2 and 4 in the ligand and in both complexes (Table 1).
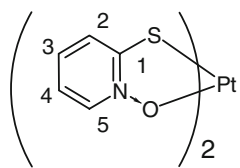
Electrochemical behavior

The redox behavior of Pt(mpo)$_2$ and Pd(mpo)$_2$ was exhaustively investigated by means of cyclic voltammetry in DMF solutions at a glassy carbon electrode. Cyclic voltammograms obtained at a scan rate of 0.05 V s^{-1} are compared in Fig. 2.

On the forward cathodic scan, one reduction process (indicated by "A" in Fig. 2) was observed at −1.78 V for Pt(mpo)$_2$ and at −1.43 V (indicated by "I" in Fig. 2) for Pd(mpo)$_2$. On the reverse scan, Pt(mpo)$_2$ showed one redox couple (indicated by "B" and "B′" in Fig. 2; 0.79/0.70 V)

Table 1 ^{1}H and ^{13}C NMR chemical shift values (δ) in parts per million, of the ligand and the complexes, in dimethyl-d_6 sulfoxide–D$_2$O (9:1) at 30 °C

Proton	δ_{H} (multiplicity)		$\Delta\delta^{\mathrm{a}}$	Carbon	δ_{C}		$\Delta\delta^{\mathrm{a}}$
	Ligand	Complex			Ligand	Complex	
–	–	–	–	1	167.91	157.23	−10.68
2	7.32 (d)	7.62 (d)	0.30	2	132.32	128.56	−3.76
3	6.74 (t)	7.46 (t)	0.72	3	124.02	131.64	7.62
4	6.55 (t)	7.18 (t)	0.63	4	114.66	120.23	5.57
5	7.97 (d)	8.41 (d)	0.44	5	139.04	138.73	−0.31

Proton	δ_{H} (multiplicity) complex	$\Delta\delta^{\mathrm{a}}$	Carbon	δ_{C} complex	$\Delta\delta^{\mathrm{a}}$
–	–	–	1	154.00	−13.91
2	7.82 (d)	0.50	2	128.68	−3.64
3	7.48 (t)	0.74	3	132.43	8.41
4	7.07 (t)	0.52	4	120.10	5.44
5	8.45 (d)	0.48	5	138.11	−0.93

Multiplicity: *d* doublet, *t* triplet

$^{\mathrm{a}}$ $\Delta\delta = (\delta_{\mathrm{complex}} - \delta_{\mathrm{ligand}})$

Fig. 2 Comparative voltammograms of Pt(mpo)$_2$ (*solid line*) and Pd(mpo)$_2$ (*dashed line*), where mpo is 2-mercaptopyridine *N*-oxide, in dimethylformamide solutions, at $v = 0.05$ V s^{-1}

and Pd(mpo)$_2$ exhibited one oxidation peak (indicated by "II" in Fig. 2) at 1.10 V. These last processes were also present when an initial potential sweep was applied towards positive values, indicating that they are independent of the reduction path.

The effect of the scan rate on the electrochemical response was investigated between 0.01 and 1 V s^{-1}. Some aspects of the results are commented on in the following sections.

Pt(mpo)$_2$

The cathodic peak (indicated by "A" in Fig. 2) shifted to more negative values as a function of v and the separation between the peak and the half-peak potential ($E_{\mathrm{pc}} - E_{\mathrm{p/2}}$) of 90 mV was independent of v. Values of

($E_{\mathrm{pc}} - E_{\mathrm{p/2}}$) greater than 56.5/$n$ mV are diagnostic of an irreversible charge transfer. In addition, the linear dependence of E_{pc} with log v and the absence of the reverse oxidation peak up to 1 V s^{-1} confirmed the irreversibility of this process.
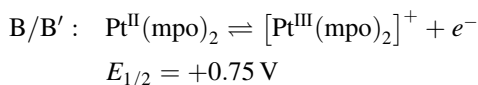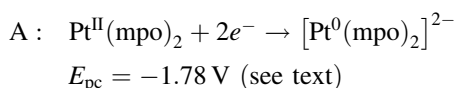
Figure 3 shows the behavior of the redox couple B/B′, which was separately investigated within a restricted potential range. The anodic and catodic peak potentials, (E_{pa}) and (E_{pc}), were dependent on v and the ΔE_{p} values were larger than the 59/n mV expected for a reversible charge transfer process [49]. Nevertheless, this behavior could be attributed to some uncompensated solution resistance, as the internal standard Fc/Fc^{+} gave similar ΔE_{p}. The $i_{\mathrm{pa}}/v^{1/2}$ value was invariant with changing scan rates and the ratio of cathodic to anodic peak currents ($i_{\mathrm{pc}}/i_{\mathrm{pa}}$) remained near unity, indicating that the oxidation product was stable during the required time for the measurements. The peak width parameter ($E_{\mathrm{p}} - E_{\mathrm{p/2}}$) of 58 mV obtained at scan rates up to 0.25 V s^{-1} was close to that predicted for a reversible diffusion-controlled process (56.5/n mV). From the average value of the anodic and cathodic peaks, at the slower scan rates, an $E_{1/2}$ value of approximately +0.75 V was determined for this process.

According to the experimental data, the metal center of the original compound could be reduced and oxidized at the potential mentioned. No evidence of chemical reactions either preceding or following the electrode process was detected [49, 50]. In addition, the current of reduction peak A was approximately twice as large as the current of
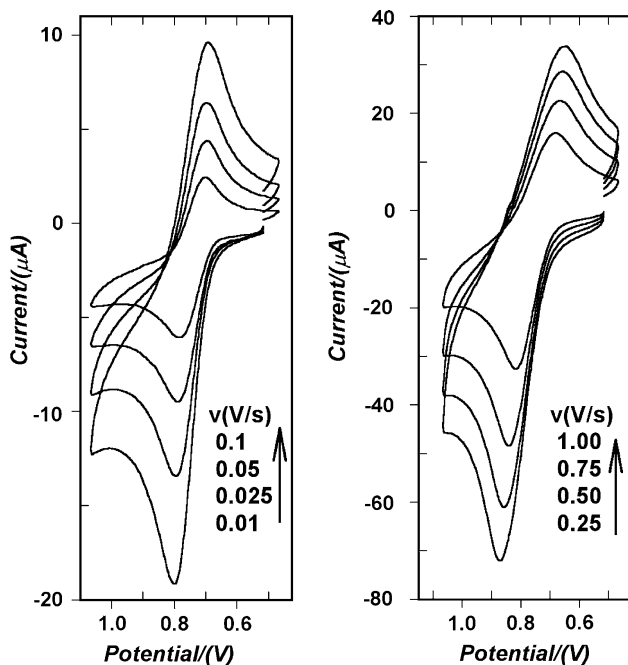
Fig. 3 Cyclic voltammograms of Pt(mpo)$_2$, in the potential range of couple B/B′, at different scan rates

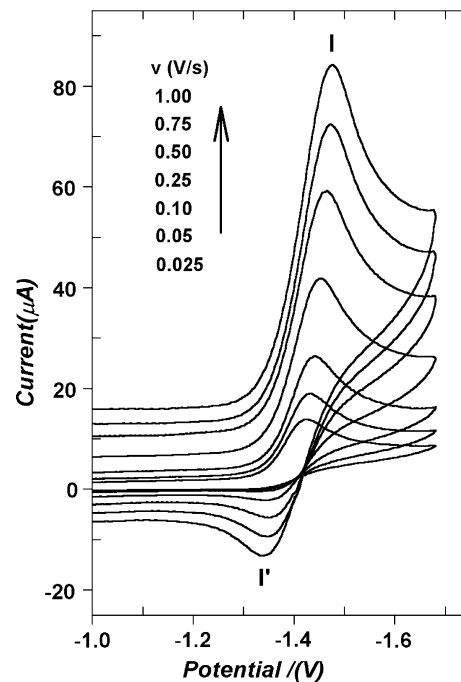**Fig. 4** Cyclic voltammograms of Pd(mpo)$_2$, between -1.00 and -1.75 V, at different scan rates

oxidation peak B [$i_p(A)/i_p(B) = 1.75$], suggesting that the irreversible process involved double the number of electrons as the reversible one. Thus, both redox processes could be formulated as follows:

A : $\mathrm{Pt^{II}(mpo)_2} + 2e^- \rightarrow \left[\mathrm{Pt^0(mpo)_2}\right]^{2-}$

$\quad\quad E_{pc} = -1.78$ V (see text)

B/B′ : $\mathrm{Pt^{II}(mpo)_2} \rightleftharpoons \left[\mathrm{Pt^{III}(mpo)_2}\right]^+ + e^-$

$\quad\quad E_{1/2} = +0.75$ V

Pd(mpo)$_2$

Figure 4 illustrates the cyclic-voltammetric behavior of this compound at different scan rates between -1.00 and -1.75 V as potential limits.

As in the previous case only one reduction peak (I) was displayed on the first cathodic scan, which was shifted to more negative values with increasing v. However, in contrast to the behavior of the platinum compound, one oxidation peak (I′) appeared on the reverse scan, at $v \geq 0.05$ V s^{-1}, which became more pronounced at increasing scan rates. Thus, the oxidation current increased with v and, consequently, the peak ratio, i_{pa}/i_{pc} increased (it was less than 1 at low v and gradually tended to unity). Moreover, the $i_{pc}/v^{1/2}$ ratio was virtually independent of the sweep rate. This behavior is indicative of a coupled chemical reaction following the electron transfer process (EC mechanism) [49–51] that is observable because the

half-life of the chemical reaction becomes comparable to the time scale of the experiment.

From the measurements, we could not determine unambiguously the number of electrons involved in this process. However, from the peak width parameter (58 ± 6 mV) and the shift of peak I towards negative potentials, which was about 30 mV for a tenfold increase in v, we could deduce that this reduction involved only one electron (theoretical value for an EC mechanism is 30/n mV) [49–51]. By comparison with the results obtained with the platinum compound, we assume that this process corresponded to a metal-centered reduction to Pd(I), followed by a chemical reaction to unidentified products. The products of this chemical reaction were not electroactive in the potential range between +1.25 and -1.75 V. Moreover, for this complex no oxidation of the metallic center was observed. The irreversible oxidation peak (II) at 1.10 V (Fig. 2) should correspond to a ligand-centered process, as it lay in a similar potential as in other metal compounds with this ligand [52]. In addition, it showed behavior analogous to that observed for the free ligand in similar experimental conditions.

Free-radical production studied by ESR spectroscopy

Electrochemical reductions of mpo and its complexes were performed in situ in DMSO solutions, applying a potential corresponding to the peak obtained from the voltammetric

experiments using the dropping-mercury electrode (see "Materials and methods"). All the compounds investigated formed stable paramagnetic intermediates at that first reduction step that were characterized by ESR.

The interpretation of the ESR by means of a simulation process confirmed the stabilities of these radical species due to the delocalization of the unpaired electron. The simulation of the spectra of mpo was made using hyperfine coupling constants obtained from the density functional theory calculations, modifying the line width, modulation amplitude and Lorentzian/Gaussian component until the spectra obtained had the greatest similarity to the experimental ones. Figure 5a shows the ESR spectrum of the mpo radical. This hyperfine pattern was simulated in terms of one triplet of the nitrogen of mpo and two doublets assigned to the hydrogen atoms belonging to the aromatic ring. The palladium and platinum complexes showed the same hyperfine pattern; however, the hyperfine constants were smaller than those of the mpo radical (Fig. 5b, Table 2).

In vitro anti-*T. cruzi* activity

The existence of an epimastigote-like form of *T. cruzi* as an obligate transitional mammalian intracellular stage has been confirmed recently [53] reinforcing the use of epimastigote cultures to evaluate the ability of drugs to inhibit the parasite growth [35]. Therefore, compounds were tested in vitro against the epimastigote form of the parasite. The ligand and both complexes were evaluated for their anti-*T. cruzi* activities against epimastigotes of Tulahuen 2 strain. The IC$_{50}$ values obtained from dose–response curves are given in Table 3.

The three compounds showed very high anti-*T. cruzi* activities (in the nanomolar range). Both complexes are between 39 and 115 times more active than the antitrypanosomal drug Nfx. In addition, as a result of

Table 2 Hyperfine coupling constants of mpo, Pt(mpo)$_2$ and Pd(mpo)$_2$ and *g* values

	N (G)	H (G)	H (G)	*g*
mpo (experimental)	1.5	15.0	15.0	2.015
mpo (theoretical)	1.3	12.0	10.8	–
Pt(mpo)$_2$	0.2	2.5	2.5	2.055
Pd(mpo)$_2$	0.2	2.4	2.4	2.050

mpo 2-mercaptopyridine *N*-oxide

Table 3 In vitro biological activity of the free ligand and its palladium and platinum complexes and comparison of 50% inhibitory concentration (IC$_{50}$) values for the parasite and for macrophages

Compound	IC$_{50}$ *Trypanosoma cruzi* (μM)	IC$_{50}$ macrophages (μM)	Selectivity index[a]
Na mpo	0.190 ± 0.015	0.85	4.5
Pd(mpo)$_2$	0.067 ± 0.015	0.33	4.9
Pt(mpo)$_2$	0.200 ± 0.018	≫2.0	≫10
Nifurtimox	7.700 ± 0.500	–	–

[a] IC$_{50}$(macrophages)/IC$_{50}$(*T. cruzi*)

coordination, the palladium complex showed approximately a threefold enhancement of the activity compared with the parent compound.

Cytotoxicity on macrophages

In order to check the specificity of the antiprotozoa activity, unspecific cytotoxic activity against mammalian cells was tested on J774 macrophages. The results are gathered in Table 4, unspecific activity being expressed as the cytotoxicity percentage, i.e., the percentage of cells that died after incubation with the compound in the
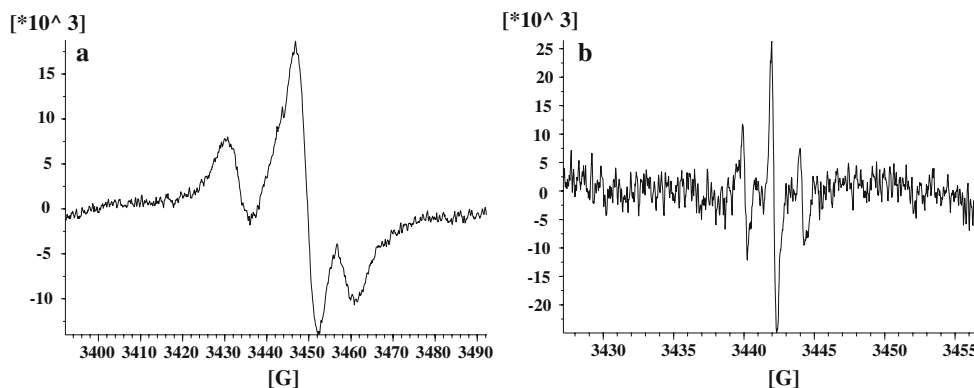
Fig. 5 **a** Experimental electron spin resonance (ESR) spectrum of the anion radical of mpo in dimethyl sulfoxide (*DMSO*). **b** Experimental ESR spectrum of the anion radical of Pt(mpo)$_2$ in DMSO. The spectrometer parameters were as follows: microwave frequency, 9.72 GHz; microwave power, 20 mW; modulation amplitude, 0.98 G; receiver gain, 59 dB

Table 4 Unspecific cytotoxic activity against macrophages expressed as cytotoxicity percentages

Compound	Doses ($\mu g\ mL^{-1}$)					
	1	0.5	0.25	0.1	0.05	0.025
Na mpo	84.8 (0.6)	74.6 (0.6)	67.5 (0.8)	41.0 (0.6)	35.8 (1.5)	5.4 (1.8)
Pd(mpo)$_2$	97.5 (0.1)	94.6 (0.1)	80.9 (0.4)	39.7 (0.9)	35.4 (0.8)	0 (2.5)
Pt(mpo)$_2$	6.6 (1.3)	0 (3.5)	0 (1.6)	0 (1.5)	0 (3.2)	0 (0.8)

Standard deviations are included in *parentheses*

specified concentration. Standard deviations are shown in parentheses.

The complexes did not show appreciable unspecific cytotoxicity on macrophages at the doses that are relevant for the anti-*T. cruzi* activity. The palladium complex and free ligand showed similar cytotoxicity on macrophages, while the platinum complex showed very low cytotoxicity towards these cells in the conditions tested.

The comparison of the anti-*T. cruzi* efficacy and the cytotoxicity against normal cells (Table 3) reveals that platinum complexation provides a higher selectivity, with the complex being preferentially toxic towards parasites besides being less toxic to the normal cells than the free ligand and the analogous palladium complex.

DNA interaction studies

In order to address if interaction with DNA could be part of the mode of action of the complexes, experiments with plasmid DNA were carried out using agarose gel electrophoresis. This approach not only enables the detection of the existence of interaction with DNA but also reveals the putative mechanisms involved through the visualization of DNA modifications that could be introduced by the metal complexes such as the appearance of single-strand nicks, which unravel the supercoiled form (form I) rendering the relaxed circular form (form II), and/or the existence of further scission events yielding a linear form (form III). In addition, the appearance of conformational changes due to the formation of anomalous structures, inducing the withdrawal of negative supercoils, promotes a reduced shift migration that can be readily visualized in native gel electrophoresis [37]. For the detection of effects on DNA due to interaction with the complexes, experiments were performed in the presence or absence of ethidium bromide. In the presence of ethidium bromide nicks would be detected. Experiments performed in its absence would allow detection of changes in the mobility of supercoiled DNA. None of these effects were evident after incubation of plasmid DNA with each mpo complex in molar ratios of metal to DNA base pairs, r_i, ranging from 0.5 to 4.0 (Fig. S1).

The results are in agreement with the spectrometric analysis of interaction with CT DNA. Indeed no significant

interaction of the metal complexes with DNA could be detected even after 96 h of incubation.

The results of these two approaches strongly suggest that DNA does not constitute an important target for the mpo complexes currently tested.

Capacity of derivatives to generate free-radical species in *T. cruzi*

Mpo and the complexes obtained were incubated with the epimastigote form of *T. cruzi* Dm28c strain in the presence of DMPO as a spin-trapping agent in order to detect possible intracelullar free-radical species. The results are shown in Fig. 6. As a positive control, a nitrofuran derivative which produces redox cycling in *T. cruzi* was included [54]. In the same experimental conditions OH• radical was detected for this compound (Fig. 6, top). Nevertheless, no ESR signal was observed either for mpo or for the palladium or platinum complexes. So, a
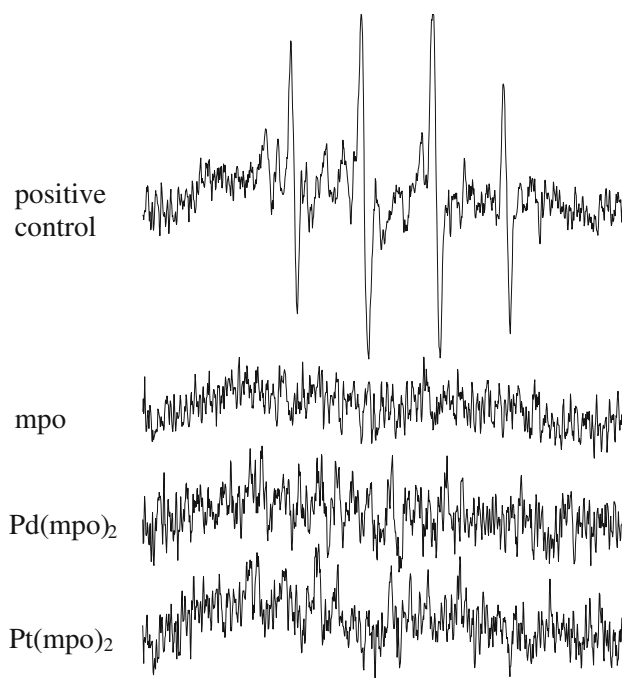
Fig. 6 ESR spectra obtained, in the experimental conditions indicated in the text, in the presence of 5,5-dimethyl-1-pirroline *N*-oxide added in order to trap free-radical species having short half-lives

bioreductive mechanism of action with participation of the compounds studied in redox cycling processes could be discarded.

Free radical scavenger capacity

Because mpo and its metal complexes are cyclic nitrones we could speculate that these compounds could act as free radical scavenger agents. In fact, the antioxidant ability of mpo has been previously demonstrated by other techniques [17]. Trying to get insight into the effect of metal coordination on the biological properties of the mpo ligand, we further evaluated the free radical scavenger activities of mpo and its metal complexes using the ORAC assay with ROO• species. Mpo showed better scavenger properties than Trolox (2.56 ± 0.182 Trolox equivalents, concentration range 0.5–2.0 μM, $r^2 = 0.9870$). Nevertheless, no effect was observed for the metal–mpo complexes in the same experimental conditions. Metal coordination substantially modified this biological property of the free ligand.

T. cruzi TR inhibition

The use of 100 μM free ligand did not produce any inhibition of TR. Unfortunately, both metal–mpo complexes were not soluble enough in aqueous solutions, preventing reliable enzyme kinetics. In general, the concentration of inhibitor is limited by the amount of DMSO, which should not exceed 50 μL per 1 mL assay because otherwise the enzyme is inhibited by the solvent. At the highest achievable concentration of 20 μM, Pd(mpo)$_2$ did not inhibit TR. At 4 and 8 μM, Pt(mpo)$_2$ also did not have any effect, but at 20 μM a 10% inhibition of TR was found. Higher concentrations of the compound could not be tested [55].
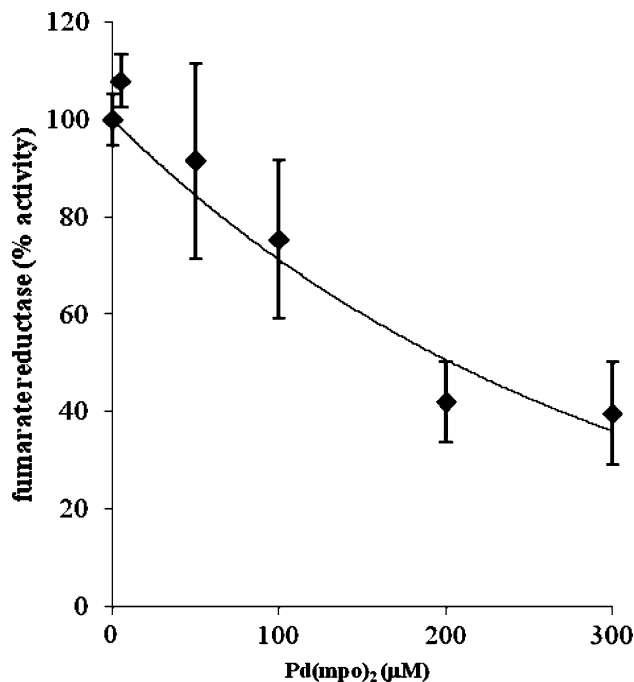
T. cruzi NADH-fumarate reductase inhibition

Since it was demonstrated that mpo is a fumarate reductase inhibitor effective on *T. cruzi* epimastigotes [16] we analyzed the effect of the palladium and platinum complexes on this enzyme activity. The results of the inhibition test at a single dose (225 μM) are shown in Fig. 7. In the conditions assayed, the free ligand and both metal–mpo complexes inhibited *T. cruzi*'s NADH-fumarate reductase. At this dose Pd(mpo)$_2$ showed the highest inhibition. While the inhibition observed for Pt(mpo)$_2$ is similar to that obtained with the ligand alone, Pd(mpo)$_2$ shows a marked increase in the inhibitory effect with respect to that of the free ligand. Interestingly similar behavior was observed when analyzing the IC$_{50}$ values of this compound for *T. cruzi* epimastigotes.

In order to further characterize the enzyme inhibition by metal–mpo complexes, the dependence of the inhibitory
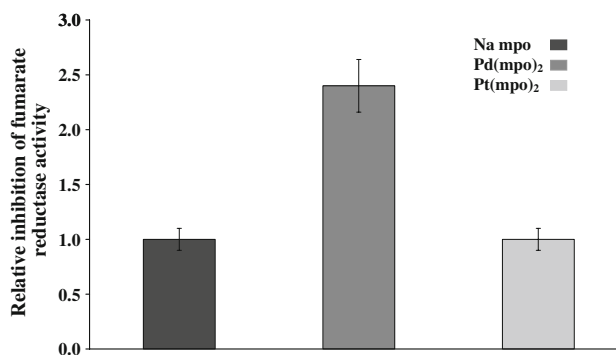

Fig. 7 Inhibitory effect of metal–mpo complexes and the sodium salt of mpo (*Na mpo*) on *Trypanosoma cruzi* NADH-fumarate reductase activity. Protein extracts of *T. cruzi* epimastigotes were incubated for 5 min at 30 °C in the absence (control) or presence of 225 μM Na mpo, Pd(mpo)$_2$ and Pt(mpo)$_2$ prior to the spectrophotometrical measurement of NADH-fumarate reductase activity as described in "Materials and methods." The total enzyme inhibition produced by Na mpo was used to calculate the relative fold of inhibition produced by Pd(mpo)$_2$ and Pt(mpo)$_2$. The standard deviation for each compound is shown as *error bars*

Fig. 8 Inhibitory effect of Pd(mpo)$_2$ on NADH-fumarate reductase from *T. cruzi* Dm28c epimastigotes. Protein extracts were incubated with various concentrations of Pd(mpo)$_2$ for 5 min at 30 °C prior to the spectrophotometrical measurement of NADH-fumarate reductase activity as described in "Materials and methods." Each point represents the average $\pm$ the standard deviation of two independent experiments run with different enzyme preparations

effect on concentration was studied for the most potent inhibitor, Pd(mpo)$_2$ (Fig. 8). The results showed that Pd(mpo)$_2$ inhibits the enzyme in a dose-dependent manner.

The supplementation of the culture medium with succinate, the product of fumarate reductase activity, to
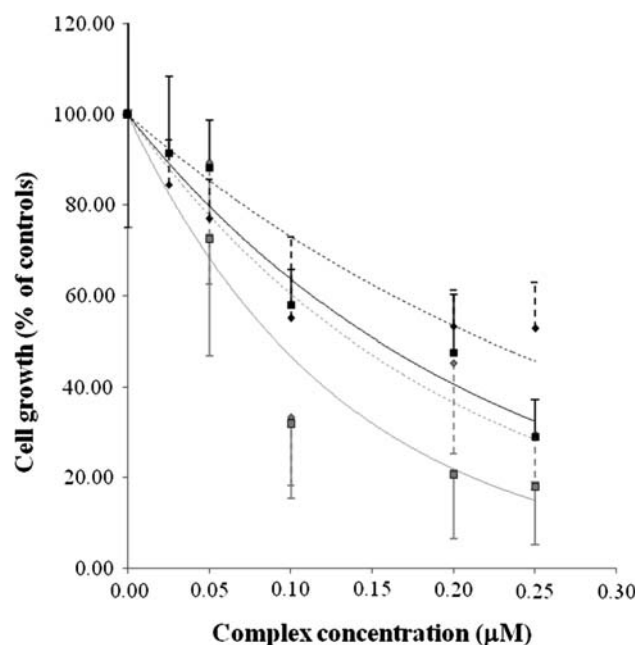
Fig. 9 Protective effect of succinate on the survival of *T. cruzi* Dm28c epimastigote cultures incubated with various concentrations of Pd(mpo)$_2$ and Pt(mpo)$_2$. The proportion of cell growth in the presence of Pd(mpo)$_2$ (*squares*) and of Pt(mpo)$_2$ (*diamonds*) supplemented with 5 mM succinate is shown. The *solid black line* represents Pd(mpo)$_2$ and the *dotted black line* represents Pt(mpo)$_2$. The *solid gray line* and the *dotted gray line* represent cells exposed to Pd(mpo)$_2$ and Pt(mpo)$_2$, respectively, in the absence of succinate. The results represent averages ± the standard deviation for three independent experiments.

alleviate the growth inhibition produced by drugs on *T. cruzi* epimastigotes has been used to prove the involvement of fumarate reductase in their mechanism of action [16]. In order to demonstrate that the growth inhibition produced by Pd(mpo)$_2$ and Pt(mpo)$_2$ was caused, at least in part, by their effect on fumarate reductase activity, *T. cruzi* epimastigotes were cultured for 5 days in the presence or absence of 5 mM succinate. A clear relief of the growth inhibition produced by both metal–mpo complexes was observed in the presence of succinate (Fig. 9).

Though we cannot discard the possibility that these metal–mpo complexes could be affecting other processes contributing to the blockage of *T. cruzi*'s growth, they clearly have an inhibitory effect on NADH-fumarate reductase.

Conclusions

Palladium and platinum complexes of the bioactive ligand mpo showed high antitrypanosomal activity with an adequate selectivity index (mammalian cells versus parasite). Coordinating mpo to Pd(II) leads to a threefold activity increase with respect to the activity of the free ligand. On the other hand, the Pt(II)–mpo complex

showed a higher selectivity for the parasite cells than that did the free ligand and the palladium analogue. NADH-fumarate reductase, as a main known parasite target for the free ligand, together with three other possible targets, namely, reductive metabolism (intraparasite free-radical production), TR and DNA, were screened to try to get insight into the mechanism of action of these metal compounds. All the data strongly suggest that the trypanocidal action of the complexes could mainly rely on the inhibition of the parasite-specific enzyme NADH-fumarate reductase. In conclusion, the results showed that both complexes have the interesting feature of acting on a parasite-specific enzyme, with only a very low dose (in the nanomolar range) being required to inhibit *T. cruzi* growth in culture. In addition, Pt(mpo)$_2$ presented lack of toxicity towards mammalian cell cultures at the doses assayed. Obviously, other biological properties of the free ligand could also have been modified through metal coordination, as shown for the free radical scavenger capacity. The results of this work show that the approach of coordinating antitrypanosomal organic compounds with pharmacologically interesting metals could be a suitable strategy to develop novel therapeutic tools against tropical diseases produced by trypanosomatids, particularly American trypanosomiasis.

References

1. http://www.who.int./ctd/chagas
2. Engels D, Savioli L (2006) Trends Parasitol 22:363–366
3. Urbina J (2003) Expert Opin Ther Pat 13:661–669
4. Cerecetto H, González M (2002) Curr Topics Med Chem 2:1185–1190
5. Krauth-Siegel RL, Bauer H, Schirmer RH (2005) Angew Chem Int Ed 44:690–715
6. Croft S, Barret M, Urbina J (2005) Trends Parasitol 21:508–512
7. Ceaser M (2005) Lancet Infect Dis 5(8):470–471
8. Yamagata Y, Nakagawa J (2006) Adv Parasitol 61:129–165
9. Zhang C, Lippard S (2003) Curr Opin Chem Biol 7:481–489
10. Farrell N (2003) Compr Coord Chem II 9:809–840
11. Sánchez-Delgado RA, Anzellotti A, Suárez L (2004) In: Sigel H, Sigel A (eds) Metal ions in biological systems, vol 41. Marcel Dekker, New York, pp 379–419
12. Sánchez-Delgado RA, Anzellotti A (2004) Mini Rev Med Chem 4:23–30
13. Chibale K (2002) ARKIVOC IX, pp 93–98
14. Urquiola C, Vieites M, Aguirre G, Marín A, Solano B, Arrambide G, Lavaggi ML, Torre MH, González M, Monge A, Gambino D, Cerecetto H (2006) Bioorg Med Chem 14:5503–5509

15. Otero L, Vieites M, Boiani L, Denicola A, Rigol C, Opazo L, Olea-Azar C, Maya JD, Morello A, Krauth-Siegel RL, Piro OE, Castellano E, González M, Gambino D, Cerecetto H (2006) J Med Chem 49:3322–3331
16. Turrens JF, Newton CL, Zhong L, Hernández FR, Whitfield J, Docampo R (1999) FEMS Microbiol Lett 175:217–221
17. Tobin D, Arvanitidis M, Bisby RH (2002) Biochem Biophys Res Commun 299:155–159
18. Cerecetto H, González M (2001) Mini Rev Med Chem 1:219–231
19. Gómez-Quiroga A, Navarro-Ranninger C (2004) Coord Chem Rev 248:119–133
20. Hall MD, Hambley TW (2002) Coord Chem Rev 232:49–67
21. Hambley TW (1997) Coord Chem Rev 166:181–223
22. Bonse S, Richards JM, Ross SA, Lowe G, Krauth-Siegel RL (2000) J Med Chem 43:4812–4821
23. Lowe G, Droz AS, Vilaiyan T, Weaver GW, Tweedale L, Pratt JM, Rock P, Yardley V, Croft SL (1999) J Med Chem 42:999–1006
24. Croft SL (1999) Mem Inst Oswaldo Cruz 94:215–220
25. Shames SL, Fairlamb AH, Cerami A, Walsh CT (1985) Science 227:1485–1487
26. Schmidt A, Krauth-Siegel RL (2002) Curr Top Med Chem 2:1239–1259
27. Parajón-Costa BS, González-Baró AC, Baran EJ (2002) Z Anorg Allg Chem 628:1419–1424
28. Shi JC, Wen TB, Zheng Y, Zhong SJ, Wu DX, Liu QT, Kang BS, Wu BM, Mak TCW (1997) Polyhedron 16:369–375
29. Davidson JL, Preston PN, Russo MV (1983) J Chem Soc Dalton Trans 783–786
30. Zhou J, Li Y, Liu Z, Chen X-T (2005) Acta Crystallogr Sect E61:m195–m197
31. Koepp HM, Went H, Strehlow HZ (1960) Z Elektrochem 64:483–491
32. Gagné RR, Koval CA, Lisensky GC (1980) Inorg Chem 19:2854–2855
33. Rigol C, Olea-Azar C, Mendizábal F, Otero L, Gambino D, González M, Cerecetto H (2005) Spectrochim Acta A 61:2933–2938
34. Huang L, Lee A, Ellman JA (2002) J Med Chem 45:676–684
35. Arán VJ, Ochoa C, Boiani L, Buccino P, Cerecetto H, Gerpe A, González M, Montero D, Nogal JJ, Gómez-Barrio A, Azqueta A, López de Ceraín A, Piro OE, Castellano EE (2005) Bioorg Med Chem 13:3197–3207
36. Mahnken RE, Billadeau MA, Nikonowicz EP, Morrison H (1992) J Am Chem Soc 114:9253–9265
37. Otero L, Smircich P, Vieites M, Ciganda M, Cardoso Severino P, Terenzi H, Cerecetto H, Gambino D, Garat B (2007) J Inorg Biochem 101:74–79
38. Ausubel FM, Brent R, Kingston RE, Moore DD, Seidman JG, Smith JA, Struhl K (1999) Short protocols in molecular biology: a compendium of methods from current protocols in molecular biology. Wiley, New York
39. Ou B, Hampsch-Woodill M, Prior RL (2001) J Agric Food Chem 49:4619–4926
40. Dávalos A, Gómez-Cordovés C, Bartolomé B (2004) J Agric Food Chem 52:48–54
41. Jockers-Scherübl MC, Schirmer RH, Krauth-Siegel RL (1989) Eur J Biochem 180:267–272
42. Denicola A, Rubbo H, Prodanov E, Turrens JF (1992) Mol Biochem Parasitol 54:43–50
43. Contreras VT, Araujo-Jorge TC, Bonaldo MC, Thomaz N, Barbosa HS, Meirelles de NM, Goldenberg S (1988) Mem Inst Oswaldo Cruz 83(1):123–133
44. Christmas PB, Turrens JF (2000) FEMS Microbiol Lett 183:225–228
45. Lin-Vien D, Colthup NB, Fateley WG, Grasselli JG (1999) The handbook of infrared and Raman characteristic frequencies of organic molecules. Academic Press, Boston
46. Tsagkalidis W, Rodewald D, Rehder D, Vergopoulos V (1994) Inorg Chim Acta 219:213–215
47. Vieites M, Gambino D, González M, Cerecetto H, Tarulli SH, Quinzani OV, Baran EJ (2006) J Coord Chem 59(1):101–106
48. Gambino D, Otero L, Vieites M, Boiani M, González M, Baran EJ, Cerecetto H (2007) Spectrochim Acta A Mol Biomol Spect 68:341–348
49. Bard AJ, Faulkner LR (2001) Electrochemical methods: fundamentals and applications, 2nd edn. Wiley, New York
50. Nicholson RS, Shain I (1964) Anal Chem 36:706–723
51. Brown ER, Large RF (1971) In: Weisberger A, Rositer BW (eds) Part IIA, Chapter 6. Interscience, New York
52. Chen X, Hu Y, Wu D, Weng L, Kang B (1991) Polyhedron 10:2651–2657
53. Tyler KM, Engman DM (2001) Int J Parasitol 31:472–480
54. Otero L, Maya JD, Morello A, Rigol C, Barriga G, Rodriguez J, Folch C, Norambuena E, González M, Olea Azar C, Cerecetto H, Gambino D (2008) Med Chem 4:119–126
55. Krauth-Siegel RL. Personal communication